URSI-B EMTS 2025, Bologna, 23–27 June

High-Q Metasurface-Enabled Cavities with Effective Electric and Magnetic Surface Impedances

Pietro Brugnolo, Samel Arslanagić and Rasmus E. Jacobsen
Department of Space Research and Technology, Technical University of Denmark, 2800 Kgs. Lyngby, Denmark,
pietrobrugnolo.pk@gmail.com, saar@dtu.dk, rajac@dtu.dk

Abstract

Planar and cylindrical metasurface cavities are investigated for bound states in the continuum. Resonant cavities formed by regular mirrors, such as perfect electric conductors, require specific cavity sizes. Instead, using metasurfaces with combined magnetic and electric responses enable resonant excitation for any cavity size. Presently, the metasurfaces are modelled using effective electric and magnetic surface impedances, and it is shown that the required surface characteristics can be achieved with simple arrays of dielectric spheres. Given the canonical structure, a fully analytical approach is developed, and expressions for the surface impedance values are presented. The analytical results are compared with full wave simulations showing great agreement. The proposed metasurface cavities may be of interest for the design of filters, antennas, sensors, and nonlinear systems.

1. Introduction

Confining fields within cavities is fundamental to electromagnetic systems across optical, microwave, and radio frequencies. Traditional approaches use fully or partially closed cavities with high-quality (Q) factors to minimize energy loss. For instance, microwave cavities are fully enclosed metallic structures, while optical Fabry-Pérot interferometers use partially closed mirrors.

An alternative is open structures supporting quasi-bound states in the continuum (quasi-BICs) [1-3]. These resonant states exhibit high Q-factors and localized fields with minimal radiation. While ideal BICs have infinite Q-factors, practical quasi-BICs achieve finite Q-factors due to structural losses and require precise coupling with external waves. Such states are common in periodic photonic structures [1, 2] and epsilon-near-zero (ENZ) materials [4]. Recently, BICs have also been demonstrated in cylindrical and planar cavities with metasurfaces (MSs) acting as quasi-perfect electric conductors [5, 6]. However, these configurations impose strict size constraints, such as half-wavelength spacing in planar cavities or roots of cylindrical Bessel functions in cylindrical ones. This size constraint can be relaxed by including a magnetic response, on top of the electric response, to the MS.

In this work, we investigate BICs in planar and cylindrical MS cavities of arbitrary sizes, facilitated by MSs exhibiting both electric and magnetic responses, which are modelled by the MS's effective electric surface impedance (Z_e) and magnetic surface admittance (Y_m) permitting an analytical approach to the problem. The analytical expressions for the required Z_e and Y_m are presented and selected examples are presented. The realized MSs consist of arrays of dielectric spheres, which are modelled analytically. The plane wave responses of the cavities are studied, and major field enhancements are observed inside the cavities. The analytical models are compared with full wave simulations showing great agreement.

In this paper, we present the boundary conditions in Section 2, which are used to derive the analytical solution to the investigated scattering problems. Next, we show the results for the planar and cylindrical cavities in Section 3 and 4, respectively, while concluding the work in Section 5. Throughout the work, the time factor exp($j\omega t$), where ω is the angular frequency and t is the time, has been assumed and suppressed.

2. Boundary Conditions

In the absence of magneto-electric effects, the boundary conditions for a MS with effective Z_e and Y_m are [7]

$$\hat{\mathbf{n}} \times (\boldsymbol{E}_1 - \boldsymbol{E}_2) = -\frac{\boldsymbol{H}_1^{\tan} + \boldsymbol{H}_2^{\tan}}{2Y_\mathrm{m}}, \quad (1)$$

$$\hat{\mathbf{n}} \times (\boldsymbol{H}_1 - \boldsymbol{H}_2) = \frac{\boldsymbol{E}_1^{\tan} + \boldsymbol{E}_2^{\tan}}{2Z_\mathrm{e}}, \quad (2)$$

where '1' and '2' denote the regions on each side of the MS and $\hat{\mathbf{n}}$ the unit normal vector pointing from region 2 to region 1. $\boldsymbol{E}_1$ ($\boldsymbol{H}_1$) and $\boldsymbol{E}_2$ ($\boldsymbol{H}_2$) are the electric (magnetic) fields on the boundary, and 'tan' indicates the tangential component of the field.

From (1) and (2), it can be shown that even for non-zero fields in region 1, the fields in region 2 can be zero if $Z_\mathrm{e}Y_\mathrm{m}$ = 1⁄4. In this case, the MS essentially functions as a 'perfect' reflector/mirror.

3. Planar Metasurface Cavity

First, we consider a cavity in free space formed by two identical planar MSs spaced by d. The MSs are infinitely extended along the y- and z-axis, and they exhibit the effective electric surface impedance Z_e and magnetic surface admittance Y_m. The cavity is illuminated by a linearly polarized plane wave propagating along the x-axis (normal incidence). A sketch of the configuration is shown in the inset of Figure 1.

The configuration is analyzed analytically to show that BICs, appearing as concurrent zeros and poles in the amplitude coefficients of the fields in between the MSs, occur when

$$Z_e^{\pm} = j\frac{\eta}{2}\frac{\cos(kd) \pm 1}{\sin(kd)}, \quad (3)$$

$$Y_m^{\pm} = -j\frac{1}{2\eta}\frac{\sin(kd)}{\cos(kd) \pm 1}, \quad (4)$$

where η and k are the intrinsic impedance and wavenumber, respectively, of the medium in between the MSs. The plus-minus sign (±) captures the polarization independence of problem. Changing between the ± solutions correspond to changing to the other orthogonal polarization. It is noted that (3) and (4) satisfy the general condition $Z_e Y_m = 1/4$ and making field zero.

To showcase the strong field enhancement when (1) and (2) are met, we consider an empty cavity ($\eta = \eta_0$) with $d = 0.2962\lambda_0$, where λ_0 is the free-space wavelength. In this case, the BIC condition is achieved when the MSs both exhibit $Z_e = -j0.6712\eta_0$ and $Y_m = j0.3725/\eta_0$. To realize these surface properties, we employ a square array of dielectric spheres, which can be modelled analytically using the spherical particle model [8]. The spheres have the radius $r_s = 0.0872\lambda_0$ and the relative permittivity $\varepsilon_{r,s} = 36$, and the lattice constant of the array is $a_s = 0.2\lambda_0$.

The analytical and simulated normalized total magnetic field intensities along the x-axis are shown in Figure 1. The incidence magnetic field has the amplitude H_0 and is in the y-direction. The first MS is placed at $x = 0$ and the second MS at $x = d$. The simulations are done using COMSOL Multiphysics. Theoretically, the MSs should form a BIC in the cavity (with infinite Q-factor), however, as the simulated MSs is not perfect, a quasi-BIC is formed instead. For this reason, the Z_e and Y_m values used for the analytical calculations have been slightly shifted away from the BIC condition to give a better comparison with the simulated results. In Figure 1, a significant field enhancement is observed inside the cavity, whereas outside the cavity, the field is much weaker. At the center of the cavity, the field magnitude is increased by 28 dB compared to the incidence field. The Q-factor of the simulated cavity is 1700. Other cavity designs have also been investigated exhibiting higher Q-factors. These will be presented at the conference. For more details on the cylindrical MS cavity, see ref. [9].

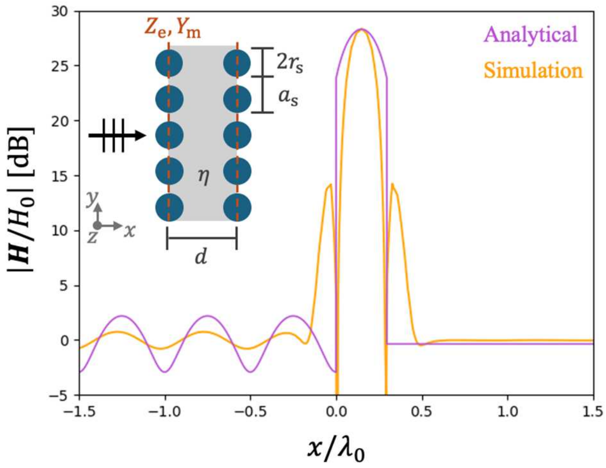

Figure 1. Planar metasurface cavity. Magnitude of the normalized total magnetic field in logarithmic scale along the x-axis. The x-coordinate is normalized with the free-space wavelength λ_0. The inset shows a sketch of the configuration.

4. Cylindrical Metasurface Cavity

Now, we consider a single MS forming a cylindrical cavity of radius r_c, which is placed in free space. As with the planar cavity investigated in Section 3, a square array of dielectric spheres is used to realize the required surface characteristics. The cylindrical MS cavity is illuminated by a transverse electric (TE) plane wave. A sketch of the configuration is included as an inset in Figure 2.

Using the classical Lorenz–Mie analysis for cylindrical harmonics (modes), analytical expressions have been derived for Z_e and Y_m, which fulfill the conditions for BICs of different cylindrical modes in the cavity

$$Z_e^{TE} = j\frac{\eta}{2}\frac{J_n'(kr_c)}{J_n(kr_c)}, \quad (5)$$

$$Y_m^{TE} = -j\frac{1}{2\eta}\frac{J_n(kr_c)}{J_n'(kr_c)}, \quad (6)$$

where J_n are the n-th order Bessel functions of the first kind with the prime denoting the derivative. Moreover, η and k are the intrinsic impedance and wavenumber, respectively, of the medium inside the cavity.

Similar to the planar case, we have found the required MS for a selected cavity size to showcase the field enhancement. For an empty cavity with $r_c = 0.7878\lambda_0$, a MS with $Z_e \approx -j0.85\eta_0$ and $Y_m \approx j0.30/\eta_0$ is needed for a BIC of mode $n = 0$. These surface impedance/admittance values can be achieved with a MS of dielectric spheres with $r_s = 0.1542\lambda_0$, $\varepsilon_{r,s} = 12.08$ and $a_s = 0.45\lambda_0$. The relative permittivity of the dielectric spheres corresponds to that of silicon at telecom frequencies. The analytical and simulated normalized total magnetic field intensities along the x-axis are shown in Figure 2. Field enhancement of around 36 dB compared to the incidence field is observed inside the cavity. The Q-factor of the simulated cavity mode is 17000. The reason for the larger Q-factor in the cylindrical cavity compared to the planar cavity, is due to smaller planar cavity size. More examples of the cylindrical cavities will be shown at the conference.

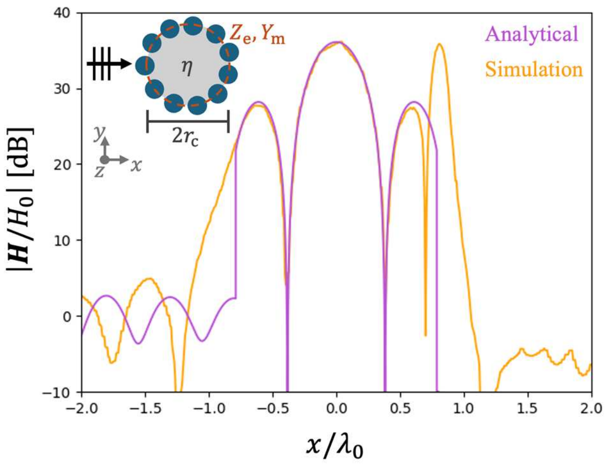

Figure 2. Cylindrical metasurface cavity. Magnitude of normalized the total magnetic field in logarithmic scale along the x-axis. The x-coordinate is normalized with the free-space wavelength λ_0. The inset shows a sketch of the configuration.

4. Conclusions

In this work, planar and cylindrical MS cavities were investigated analytically and numerically BICs. The analytical expressions for the required surface impedance and admittance of the MSs were presented. The MSs were realized by a square array of dielectric spheres. The analytical and numerical results of selected examples were presented showcasing significant field enhancement inside the cavities. More details on the analytical formulation of the MS cavity, as well as more examples, will be presented at the conference.

Although, the considered MSs in this work consists of all-dielectric materials, metals are also viable, in particular at microwave frequencies. Moreover, using reconfigurable MS will further expand the applicational perspective for the considered cavities [10, 11]. Currently, we are pursuing the possibility of an experimental demonstration of a planar cavity operating at microwave frequencies.

References

[1] C. W. Hsu, B. Zhen, A. D. Stone, J. D. Joannopoulos, and M. Soljacic, "Bound states in the continuum," *Nature Reviews Materials*, September 2016, **1**, 9, p. 16048, doi: 10.1038/natrevmats.2016.48.

[2] K. Koshelev, G. Favraud, A. Bogdanov, Y. Kivshar, and A. Fratalocchi, "Nonradiating photonics with resonant dielectric nanostructures," *Nanophotonics*, **8**, 5, May 2019, pp. 725–745, doi: 10.1515/nanoph-2019-0024.

[3] A. F. Sadreev, "Interference traps waves in an open system: bound states in the continuum," *Reports on Progress in Physics*, **84**, 5, April 2021, p. 055901, doi: 10.1088/1361- 6633.

[4] F. Monticone, et al., "Trapping light in plain sight: embedded photonic eigenstates in zero-index metamaterials," *Laser & Photonics Review*, **12**, 5, May 2018, p. 1700220, doi: 10.1002/lpor.201700220.

[5] F. S. Cuesta, V. S. Asadchy, A. D. Sayanskiy, V. A. Lenets, M. S. Mirmoosa, X. Ma, S. B. Glybovski, and S. A. Tretyakov, "Nonscattering metasurface-bound cavities for field localization, enhancement, and suppression," *IEEE Transaction on Antennas and Propagation*, **68**, 3, March 2020, pp. 1689-1703, doi: 10.1109/TAP.2019.2938661.

[6] R. E. Jacobsen and S. Arslanagić, "Extreme localization of fields in open cylindrical impedance surface cavities," *IEEE Transaction on Antennas and Propagation*, **72**, 2, February 2024, pp. 1686-1693, doi: 10.1109/TAP.2024.3349783

[7] C. Pfeiffer and A. Grbic, "Bianisotropic metasurfaces for optimal polarization control: Analysis and synthesis," *Physical Review Applied*, **2**, October 2014, p. 044011, doi: 10.1103/PhysRevApplied.2.044011

[8] A. Monti, A. Alu`, A. Toscano, and F. Bilotti, "Surface impedance modeling of all-dielectric metasurfaces," *IEEE Transactions on Antennas and Propagation*, **68**, 3, March 2020, pp. 1799-1811, doi: 10.1109/TAP.2019.2951521

[9] P. Brugnolo, S. Arslanagić, and R. E. Jacobsen, "Bound States in the Continuum in Cylindrical All-Dielectric Metasurface Cavities," Physical Review Letters, in press.

[10] R. E. Jacobsen, A. V. Lavrinenko, and S. Arslanagić, "Reconfigurable dielectric resonators with imbedded impedance surfaces—From enhanced and directional to suppressed scattering," *Applied Physics Letters*, **122**, 8, February 2023, p. 081701, doi: 10.1063/5.0139695

[11] O. Tsilipakos, A. C. Tasolamprou, A. Pitilakis et al., "Toward Intelligent Metasurfaces: The Progress from Globally Tunable Metasurfaces to Software-Defined Metasurfaces with an Embedded Network of Controllers," *Advanced Optical Materials*, **8**, 17, September 2020, p. 202000783. doi: 10.1002/adom.202000783.